Control and Prevent Land Subsidence Caused by Foundation Pit Dewatering in a Coastal Lowland Mega City: Indicator Definition, Numerical Simulation and Regression Analysis

Jianxiu Wang (wang_jianxiu@163.com)
Tongji University College of Civil Engineering https://orcid.org/0000-0001-5438-8184
Tianliang Yang
Shanghai Institute of Geological Survey
Guotao Wang
Tongji University
Xiaotian Liu
Tongji University
Na Xu
Tongji University
Esther Stoumather
Utrecht University: Universiteit Utrecht
Yao Yin
Tongji University
Hanmei Wang
Shanghai Institute of Geological Survey
Xuexin Yan
Shanghai Institute of Geological Survey
Xinlei Huang
Shanghai Institute of Geological Survey

Research Article

Keywords: costal lowland city, foundation pit dewatering (FPD), 3H subsidence and drawdown indicator, numerical simulation, regression analysis

Posted Date: January 13th, 2022

DOI: https://doi.org/10.21203/rs.3.rs-1221768/v1

Control and prevent land subsidence caused by foundation pit dewatering in a coastal lowland mega city: Indicator definition, numerical simulation and regression analysis

Jianxiu Wang[1,2,*], Tianliang Yang[3], Guotao Wang[1], Xiaotian Liu[1], Na Xu[1]，Esther Stoumather[4]，Yao Yin[1], Hanmei Wang[3], Xuexin Yan[3], Xinlei Huang[3]

[1] College of Civil Engineering, Tongji University, Shanghai, 200092, China

[2] Key Laboratory of Geotechnical and Underground Engineering of Ministry of Education, Tongji University, Shanghai, China

[3] Shanghai Institute of Geological Survey, Shanghai 200093, China

[4] Utrecht University, Utrecht 3584CB, the Netherlands

Corresponding author: *Jianxiu Wang, Department of Geotechnical Engineering, Tongji University, Shanghai 200092, China; e-mail: wang_jianxiu@163.com; Tel: +86-13916185056, +86 21 65983036.

Abstract: Coastal mega cities are often commercial centers because of convenient traffic. Safe elevation above sea level is vital for their sustainable development. Global climate change and sea level rising increase flood risk especially in the lowland subsidence area. Shanghai of China was selected as research background. Although groundwater exploitation had been strictly restrained to control land subsidence and reserve safe elevation, lowering groundwater level during underground excavation cannot be avoided. Foundation pit dewatering (FPD) was intensively performed in underground exploitation during urbanization and city renewal. The FPD settlement accelerated land subsidence. Controlling FPD subsidence was urgent.

Normally, the maximum horizontal influence radius of foundation pit excavation was less than three times excavation depth (H), and the 3H settlement was only caused by the FPD. The 3H maximum settlement was defined as the evaluating indicator of FPD land subsidence, and the corresponding 3H drawdown was defined as the control indicator of land subsidence. The FPD conceptual models were established on the basis of estimation and investigation of foundation pit information, including pit area, pit shape, pit depth, and curtain depth. Numerical models were established and a total of 5650 FPD numerical simulations were performed to investigate the land subsidence and FPD drawdown. Multi-factor regression analysis was conducted to obtain relations between land subsidence and FPD drawdown. Regression models were established between the 3H drawdown and the shape, area, depth, and curtain depth of foundation pit on the basis of the numerical simulations. A typical example introduced to verify the regression models. The regression models were used to manage the FPD land subsidence by controlling the 3H FPD drawdown. The results can provide reference for the land subsidence control in a coastal lowland city.

Key words: costal lowland city; foundation pit dewatering (FPD); 3H subsidence and drawdown indicator; numerical simulation; regression analysis

1 Introduction

Safe elevation above sea level is vital for a coastal city under global climate change and sea level rise. Land subsidence must be prevented and controlled effectively within a certain extension to reserve enough elevation in lowland areas. Lowland coastal cities often locate in a delta multi-aquifer and multi-aquitard (MAMA) system. Groundwater exploitation is normally

the most important source for the land subsidence in of the cities. Ground water exploitation can be restricted severely to control increasing land subsidence by using surface water. However, lowering groundwater level during excavation for underground space development cannot be avoided during urbanization and city renewal. It is estimated that the quantity of groundwater extracted for foundation pit dewatering (FPD) was approximately 10 times higher than groundwater exploitation in 2020 in Shanghai (Wang et al **2021**). FPD has become the dominant factors influencing land subsidence exceeding groundwater exploitation. FPD land subsidence prevention and control have become an urgent task. Waterproof curtain was often adopted to cut off dewatered aquifers in shallow foundation pits. However, some aquifers in a MAMA system were too deep to be cut off. FPD drawdown funnel caused corresponding land subsidence funnel. The land subsidence funnels developed and merged in certain spatiotemporal range forming larger land subsidence funnels.

Currently, the studies on land subsidence mainly focused on monitoring, evaluation, groundwater extraction. The studies on FPD mainly concentrate on individual FPD engineering. The management of FPD land subsidence in city scale is seldom conducted. Models evaluating and control individual FPD to realized city land subsidence control aim are rarely concerned. **Mo and Fu (2002)** proposed that the combined system dewatering method of pumping and recharge wells can effectively reduce the groundwater level of foundation pit and control the settlement of adjacent buildings. **Luo et al. (2007)** developed a 3D full coupling model between seepage and stress on the basis of Biot's consolidation theory to simulate and forecast the characteristics of groundwater seepage and land subsidence around the foundation pit of Shanghai Huanqiu Finance Center. **Hoque et al (2007)** studied the declining groundwater level

and aquifer dewatering in Dhaka metropolitan area, Bangladesh. **Miyake et al. (2008)** used multi-aquifer pumping test and finite element method to determine the insertion depth of waterproof curtain in a large-scale excavation site in Tokyo, Japan. **Wu et al. (2009), Zhang et al. (2010)** studied the subsidence in Su-Xi-Chang area of Jiangsu Province of China. **Hung et al. (2010)** monitored severe aquifer-system compaction and land subsidence in Taiwan using multiple sensors. **Shen et al (2012)** performed groundwater control for a deep excavation pit in gravel aquifer of Hangzhou, China. **Wu et al. (2015a, 2015b)** conducted a numerical investigation of the leakage behavior of cut-off walls in gravel strata caused by dewatering in a deep excavation pit. **Wang et al. (2016)** proposed that the land subsidence induced by subway FPD was divided into local and areal subsidence. The former was managed by construction organizations, and the latter was controlled by land resource, urban management, and hazard prevention department. **Wang et al. (2019)** studied the coupling effect of cut-off wall and pumping well using transparent soil laboratory experiments and indicated that the insertion depth ratio of cut-off wall effectively influences drawdown. **Zeng et al. (2018)** reported that field measurements shown that ground settlements occurred during well redevelopment. **Wang and Wang (2019)** analyzed the monitoring data of excavation and support using the deep foundation pit project in the M-1 line of Jinan Metro as the background. The maximum settlement value of the building appears at the two corners far from the foundation pit, with the value of 4.3 mm. Under field pumping test verification, numerical simulations were performed to understand the influence of dewatering on land subsidence and drawdown (**Wang et al. 2009, 2013, 2014, 2018; Nicoleta et al. 2017; Khosravi et al. 2018; Shi et al., 2018；Zhang et al. 2018**). However, most of the studies focus on single FPD engineering and cannot solve the

FPD subsidence management problems under city scale.

In the current manuscript, Shanghai was selected as research background, the subsidence at the position of three times excavation depth (3H) was defined as the evaluation indicator of FPD land subsidence under land subsidence prevention and control partition (**Shanghai 2020**). The corresponding 3H drawdown was defined as the control indicator of FPD land subsidence. A total of 5650 numerical simulations were conducted to consider the influence of foundation pit shape, area, depth and curtain depth on FPD drawdown and land subsidence. Regression analysis was performed for different partitions of the MAMA system. The threshold 3H drawdown was suggested for different MAMA partition after verified using a sample. The methods can provide reference for land subsidence control in similar lowland coastal cities.

2 FPD numerical model

2.1 Background

Shanghai is located in front of the Yangtze River Delta Plain. Except for sporadic residual volcanic rocks exposed in the southwest, all bedrocks are covered with Quaternary strata. The layers of Shanghai are composed of a typical MAMA system. The Quaternary strata in Shanghai area are divided into 16 engineering geological strata in accordance with generation time, genetic types, and main engineering geological features (Shanghai Geological Environmental Atlas, **2002**). Seven major engineering geological layers concerning FPD land subsidence are shown in Table **1**.

2.2 Landform partition

The MAMA system underlying Shanghai is not a complete, independent groundwater system but rather a part of the water systems of the Yangtze Delta. Shanghai is divided into four

111 landform partitions (Fig. **1.**), namely, lakes and marshes plain area, coastal plain area, river
112 estuary sand island area, and Tidal flat geomorphic area, in accordance with engineering
113 geological and hydrogeological conditions and MAMA combinations (Table **2**).

114 **2.3 Land subsidence prevention and control (LSPC) partition**

115 Shanghai land subsidence prevention and control partitions are shown in Fig. **1.**

116 (1) Emphasis prevention areas (Area I)

117 Area I_1: It refers to the central city area within the outer ring line. Severe land subsidence
118 disasters have occurred, which make the situation of flood control in the central city adverse.
119 The uneven land subsidence phenomenon is evident, which has a great impact on the safe
120 operation of major projects, such as rail transit. The average annual land subsidence in this
121 area should be controlled within 7 mm/a, and the groundwater level of the fourth confined
122 aquifer is restored to －12 m, further reducing the impact of differential land subsidence.

123 Area I_2: It refers to the Pudong New Area besides the Outer Ring Road and Da Hongqiao
124 Planning Area. It is a serious land subsidence area besides the central city. With the adjustment
125 and implementation of the urban master plan, the recent development of land subsidence has
126 shown an aggravating trend. Land subsidence centers, such as Hongqiao and Sanlin, have
127 been formed, and such formation has a serious impact on the safe operation of infrastructure,
128 such as rail transits and maglev trains. The average annual land subsidence in this area should
129 be controlled within 10 mm, the groundwater level is raised steadily, the impact of groundwater
130 development on regional land subsidence is reduced, and the impact of differential land
131 subsidence should be alleviated.

132 (2) Second emphasis prevention areas (Area II)

Second emphasis prevention areas include Baoshan, Jiading, and Minhang districts. The current water level of the main groundwater exploitation levels in this area is low, and the land subsidence is medium. The average annual land subsidence in this area should be controlled within 6 mm, basically eliminating the groundwater level funnel along the lifeline project.

(3) General prevention areas (Area III)

General prevention areas include Fengxian, Songjiang, Jinshan, Qingpu district, and Chongming county. Except for the new town, the overall development intensity is low, and the land subsidence belongs to the general area. However, the regional land subsidence caused by groundwater exploitation in adjacent provinces remains prominent in some areas, and the seawall on the north coast of Hangzhou Bay is sensitive to the impact of land subsidence. The average annual land subsidence in this area should be controlled within 5 mm, and the groundwater level funnel formed by groundwater exploitation in this area should be eliminated actively.

2.4 Subsidence-drawdown double control (SDDC) partition

SDDC partition was determined in accordance with partition principle shown in Table **3**. The number of each partition was divided into three levels. See Fig. **2**.

2.5 Evaluation and control indicator under SDDC partition

The excavation influence radius under retaining conditions is normally less than 3H. The subsidence with in 3H is caused by excavation and FPD which can be recovered by construction. The land subsidence outside 3H is caused by FPD which should be managed by public department. Its extension has far exceeded construction range which superposed and enlarged spatiotemporally and cannot be treated by an individual construction unit. The FPD

land subsidence should be prevented and controlled by public agency to maintain lowland city safe elevation. The land subsidence within 3H was suggested to be managed by construction manager, while the land subsidence outside 3H was suggested to be managed by government. The maximum 3H subsidence was defined as evaluation indicator for FPD land subsidence prevention and control, which was determined by the latest city land subsidence prevention plan. The maximum 3H drawdown was defined as control indicator which was determined by the threshold of corresponding evaluation indicator.

2.6 Foundation pit conceptual model

The characteristics of foundation pits in Shanghai were estimated and investigated. A total of 207 foundation pit cases were collected. The conceptual model of a foundation pit was summarized on the basis of the cases.

In the collected cases, the plane shape of the foundation pits was mostly rectangular, near rectangular, and irregular polygons (Fig. **3a**). The rectangular shapes accounted for more than half of the total number. Irregular polygons were mainly T-shaped and L-shaped which can be decomposed into rectangles. Thus, the shape of a foundation pit was determined to be represented by rectangular shapes. The length-to-width ratio (the ratio of long side to short side) was used to describe a rectangular foundation pit. The length–width ratios of the rectangle were determined as 1:1, 1.5:1, 2:1, 2.5:1, and 3:1 (Table **4**). The shape of a typical subway station foundation pit was long and narrow. It was approximately 200 m long and 15–25 m wide. Its length–width ratio was approximately 10:1.

Most of the collected foundation pits of common industrial, civil buildings, and subway stations were located in residential areas. The area of half of the cases were between 5000 and 10,000

177 m^2 (Fig. **3b**). The minimum area was approximately 300 m^2, and the maximum exceeded 5000
178 m^2. Thus, foundation pit area was determined to be ranged from 1000 m^2 to 10,000 m^2. The
179 area increment step was determined as 1000 m^2. The area of a subway station foundation pit
180 was approximately 4000 m^2.
181 Non-rectangular shaped foundation pits were converted into rectangular ones by using area
182 equivalent method. A circular foundation pit can be converted into a square foundation pit:

183 $$\pi \cdot r^2 = a^2 \qquad a = \sqrt{\pi} \cdot r \,, \tag{1}$$

184 where r is the foundation pit radius (m), and *a* is the side length of square (m).
185 The depth of foundation pit was determined on the basis of the excavation depth of industrial
186 and civil buildings, as well as subway station foundation pit. The depth of foundation pit was
187 generally 4 m per floor in accordance with the basement height of civil buildings. The depth was
188 obtained by multiplying 4 m with the number of floors. The initial depth requiring lowering ground
189 water level can be calculated through the anti-gushing calculation in each MAMA partition. Then
190 the calculation depths were summarized as 24, 32, and 36 m for two-layer, three-layer, and
191 four-layer pits, respectively.
192 The underground independent subway station in Shanghai was four to three floors underground.
193 The excavation depths of the second and third floor stations were 18 and 24 m, respectively, in
194 accordance with the statistical data of several metro stations in Shanghai.
195 The retaining structures of foundation pit in Shanghai were normally diaphragm wall, bored row
196 pile, stiff cement–soil mixing pile, gravity retaining wall dam of cement–soil mixing pile, and
197 composite soil nailing wall. Diaphragm wall was mostly suitable for the excavation of foundation
198 pits with a depth exceeding 10 m.

Considering the interaction mechanism of diaphragm wall and pumping well, the depth of the wall cut into aquifers was no less than 5 m. Thus, the increment of cut-off depth of the wall into dewatering aquifer was determined as 5 m.

The maximum diaphragm wall depth has reached 150 m in Shanghai for certain special engineering. However, the normal depth of diaphragm wall was between 60 and 65 m because of the constraints of construction technology and cost. Thus, the calculation depths of diaphragm wall were determined as 31, 36, and 41 m (second floor) and 43, 48, and 53 m (third floor).

The minimum length of the filter tubes of pumping wells was determined as 6–10 m in accordance with the statistical data and engineering experience in Shanghai.

When the bottom of cutoff wall was located in gravel soil, sand, and silt aquifer, the stability of quicksand for homogeneous aquifer and groundwater seepage was expressed as the following:

$$\frac{(2D+0.8D_1)\gamma'}{\Delta h\gamma_w} \geq K_{se}, \tag{2}$$

where K_{se} is the safety factor of quicksand and the support structure with the safety grade of one, two, and three levels and should be greater than 1.6, 1.5, and 1.4, D is the soil thickness from the bottom of the cut-off wall to the bottom of the pit (m), D_1 is the soil thickness from the top of the confined aquifer to the bottom of foundation pit (m), γ' is the effective unit weight of soil (kN/m^3), Δh is the head difference inside and outside the foundation pit (m), and γ_w is the unit weight of water (kN/m^3).

When the excavation surface was located in an aquitard overlying a confined aquifer, its anti-gushing stability should be checked by using the following equation:

$$\gamma_S P_{Wk} \le \frac{1}{\gamma_{RY}} \sum \gamma_i h_i , \quad (3)$$

where γ_s is the partial coefficient of confined water action and is set to 1.0, P_{wk} is the standard value of water pressure at the top of confined aquifer (kPa), γ_i is the weight of each soil layer from the top to the bottom of confined aquifer (kN/m^3), h_i is the thickness of soil layers from the top to the bottom of confined aquifer (m), and γ_{RY} is the coefficient of confined water and is set to 1.1.

The calculated safety factor checking anti-gushing of foundation pit floor was determined to be 1.05. In practical application, the dangerous combination of aquifer elevation and piezometric head was selected for calculation under this safety factor. For normal conditions, the safety factor was determined to be set to 1.1.

The FPD period was determined to be 90 d in accordance with the construction period of a general FPD project.

2.7 FPD mathematical model

The 3D unsteady seepage mathematical model of FPD was expressed as follows:

$$\begin{cases} \dfrac{\partial}{\partial x}\left(k_{xx}\dfrac{\partial h}{\partial x}\right)+\dfrac{\partial}{\partial y}\left(k_{yy}\dfrac{\partial h}{\partial y}\right)+\dfrac{\partial}{\partial z}\left(k_{zz}\dfrac{\partial h}{\partial z}\right)-W=\dfrac{E}{T}\dfrac{\partial h}{\partial t} \text{.....(x, y, z)} \in \Omega \\ h\left(x,y,z,t\right)\big|_{t=0}=h_0\left(x,y,z\right) \text{.....(x, y, z)} \in \Omega \\ h\left(x,y,z,t\right)\big|_{\Gamma_1}=h_1\left(x,y,z,t\right) \text{.....(x, y, z)} \in \Gamma_1 \\ \mathrm{q}\left(x,y,z,t\right)\big|_{\Gamma_2}=q_1\left(x,y,z,t\right) \text{.....(x, y, z)} \in \Gamma_2 \end{cases}, \quad (4)$$

where $E=\begin{cases} S & confined \\ S_y & unconfined \end{cases}$, $T=\begin{cases} M & confined \\ B & unconfined \end{cases}$, $S_s=\dfrac{S}{M}$, S is the water storage coefficient, S_y is the degree of water supply, M is the confined aquifer unit thickness (m), B is the saturated thickness of groundwater for the submersible aquifer unit (m), k_{xx}, k_{yy}, k_{zz} is the hydraulic conductivity in anisotropic principal direction (m/d), h is the

239 water head value of (x, y, z) at *t* moment (m), W is the source and sink $(1/d)$, h_0 is

240 the initial head value of the area (m), h_1 is the water head values for the first type of

241 boundary (m), h_2 is the water head values for the first type of boundary for the pit (m),

242 S_s is the storage $(1/m)$, t is the time (d), Ω is the calculation domain, and Γ_1 and Γ_2

243 are the first and second types of boundary.

244 When the FPD aquifer was silt or silt and sand, its subsidence was mainly instantaneous

245 elastic deformation. The additional load of soil layer caused by the decreasing groundwater

246 level can be calculated using the following:

247 $$\Delta P = \gamma_w (h_1 - h_2), \quad (5)$$

248 where ΔP is the additional load of soil layer caused by dewatering (KPa), h_1 is the

249 water head height (m) of soil layer before dewatering, h_2 is the water head height (m)

250 after water level falling, and γ_w is the water weight (kN/m^3).

251 The FPD land subsidence was calculated by using a two-step method. A stratified

252 summation method was expressed by using the following:

253 $$S = \sum_{i=1}^{n} S_i = \sum_{i=1}^{n} \frac{\Delta P_i}{E_i} H_i, \quad (6)$$

254 where S is the total additional ground settlement (m) caused by dewatering, S_i is the

255 additional soil settlement (m) calculated for layer *i*, ΔP_i is the additional load (kPa)

256 calculated for layer *i*, E_i is the compressive modulus (kPa) calculated for layer *i*, and H_i

257 is the thickness (m) calculated for layer *i*.

258 In the above formulas, elastic modulus E_i was used for sandy soil. The following formulas

259 can be used for clay and silt:

$$E_s = \frac{1+e_0}{a_v}, \quad (7)$$

where e_0 is the original void ratio of the soil layer, and a_v is the volume compressibility coefficient of the soil layer (MPa^{-1}) and should be taken as the stress section from the effective self-weight pressure of the soil to the sum of the effective self-weight pressure and additional pressure of the soil.

The following correction methods were used to correct the land subsidence:

(1) Moisture correction: the buoyancy of groundwater was reduced by multiplying the actual head with the water content.

(2) Consolidation correction: The settlement lag effect was ignored because the subsidence calculated above was the final settlement. In the actual settlement calculation, the consolidation degree of each stratum participating in the calculation should be considered. Consolidation can be calculated using the following formula:

$$U_z = 1 - \frac{8}{\pi^2} \sum_{m=1,3}^{m=\infty} \frac{1}{m^2} \exp(-\frac{m^2\pi^2}{4} \mathrm{T}_v), \quad (8)$$

$$T_v = c_v t / H^2, \quad (9)$$

where T_v is the consolidation time factor corresponding to dewatering time (3 months), c_v is the consolidation coefficient (m^2/d), t is the consolidation time (d), H is the thickness of soil layer (m), and U_z is the degree of consolidation.

(3) Modification of compressive modulus: In-situ test data should be used to correct the large deviation between the compressive modulus of natural foundation and that obtained in laboratory.

2.8 FPD numerical model

281 The maximum foundation pit area was selected as 10,000 m^2. The influence distance of the
282 largest foundation pit was selected as 2000 m, and the calculation domain was set to 4200 m
283 × 4200 m. The basic parameters of the strata are shown in Table **5**. Constant head boundary
284 in the pit was used to simulate the lowering water level.
285 A total of 11 observation wells were deployed outward on each side of the model. The horizontal
286 logging was arranged at 10, 20, 30, 50, 100, 150, 200, 300, 500, 1000, and 1500 m to the
287 boundary of foundation pit.
288 The numerical simulations were performed by using a modular 3D finite–difference
289 groundwater flow model (**McDonald and Harbaugh 1988**). The scenarios are shown in Table
290 **6**.

291 **3 Numerical results**

292 **3.1 Drawdown funnel zoning**

293 Lowering groundwater level formed drawdown funnel. FPD drawdown funnel can be divided
294 into three zones (Fig. **4**): (1) steep changing zone, (2) slow changing zone, and (3) residual
295 zone according to funnel sectional shape.
296 (1) Steep changing zone
297 This zone was defined as the area ranging from foundation pit boundary to the inflection point
298 of drawdown funnel in section. The inflection point was defined as the position where the
299 tangent slope of drawdown funnel equaled to 45°. The subsidence within the zone was large.
300 (2) Slow changing zone
301 The area ranging from inflection point to the position where drawdown equaled to nature
302 groundwater level fluctuation amplitude or 30 cm were defined as slow variation zone. The

303 settlement within the zone was middle.

304 (3) Residual zone

305 The area ranging from slow changing zone to zero drawdown point was defined as residual

306 zone. area. The subsidence within the zone was not obvious.

307 The typical time-drawdown funnels are shown in Fig. **5.**

308 **3.2 Rectangle length-width direction effect**

309 A total of 11 observation wells were arranged outside the foundation pit perpendicular to the

310 long and short sides of a rectangular foundation pit (Fig. **6**).

311 The 3H drawdown was calculated when the length–width ratio was 2:1 and area was 10,000

312 m^2 using an interpolation method. The ratio of 3H drawdown in *Y* direction to that in *X* direction

313 is shown in Table **7**.

314 The drawdown in *Y* direction was approximately 0.85–0.97 times of that in X direction. The ratio

315 increased with increasing depth of dewatered aquifer. The 3H drawdown was different when

316 the length-to-width ratio was different with same area. The larger the aspect ratio was, the larger

317 the drawdown in the long side direction was, and the smaller the drawdown in the short side

318 direction was. The land subsidence monitoring points should be arranged in *X* direction.

319 **3.3 Rectangle length–width ratio effect**

320 The 3H drawdown of a foundation pit with length-to-width ratio of 2:1 is shown in Table **8** and

321 Fig. **7**. The 3H drawdown decreased with the increasing length-to-width ratio with other factors

322 as constant. However, the variation was within 0.1 times (the relative length-to-width ratio is 2:1)

323 when the foundation pit area, excavation depth, and cut off depth remained constant. The

324 change of 3H drawdown was small. The change ⑤$_2$>⑦>⑨ when the location of the dewatered

aquifer was deep. The change of 3H drawdown was small when layers ⑦ and ⑨ were connected. The change of 3H drawdown decreased gradually with the increase of the length-to-width ratio under an exponential function rule. The length-to-width ratio had significant effect on drawdown outside pit. The effect gradually decreased with the increase of the length-to-width ratio. The depth and thickness of the dewatered aquifer were important factors affecting the length-to-width ratio effect. The regularity analysis was based on the 3H drawdown with length-width ratio of 2:1.

3.4 Foundation pit depth effect

The 3H drawdown increased with the increasing excavation depth with an approximately linear relationship when the foundation pit area, diaphragm wall depth, and aspect ratio of diaphragm wall were constant.

The 3H drawdown increased with the increase in excavation depth for same pit area. They showed an approximately linear relationship when the foundation pit area, length-to-width ratio, and depth of the diaphragm wall inserted into the aquifer remain constant. As shown in Table **9,** the influence of foundation pit depth changed when the 3H drawdown increased with the increasing dewatered aquifer depth of dewatering. For 1 m increment, the excavation depth corresponds to the increase value of drawdown: ⑨>⑦>⑤$_2$. The 3H drawdown was small when the dewatered aquifer thickness was large. The 3H drawdown showed an approximately linear function law with depth. The excavation depth had a significant impact on the 3H drawdown. The depth and thickness of the target aquifer for dewatering were important factors affecting the influence of excavation depth on the 3H drawdown.

3.5 Cutoff wall depth effect

Diaphragm wall is frequently used as FPD waterproof curtain. Its depth cutting off dewatered aquifer had an obvious influence on the 3H drawdown. At present, increasing curtain cutting off depth had become a consensus method in Shanghai. Understanding the 3H drawdown under different cut off depth was of great importance to control FPD land subsidence. The cut off depth increment was set as 5 m. The curtain belonged to partially penetrating curtain. The hydraulic barrier effect of the curtain was unremarkable when cutoff depth was 5 m. The curtain changed into an inner-wrapped type with the increasing cut off depth. The hydraulic barrier effect became significant**.**

The 3H drawdown decreased with the increasing cut off depth when other factors remain constant. (Table **10**).

The 3H drawdown decreased with the increasing cut off depth when others influence factors remain constant. The cut off depth presented an exponential function to the 3H drawdown when the dewatered aquifer thickness of dewatering was large, i.e. layer ⑦ connected with layer ⑨. The effect of cut off depth weakened when cutoff depth increased to a certain value. The cut off depth had a linear relationship with the 3H drawdown when the thickness of target aquifer was small where layers ⑦ and ⑨ were disconnected.

The above analysis results show that the penetration depth of diaphragm wall has a significant impact on the 3H drawdown. The cutoff depth effect reducing the 3H drawdown weakened when the depth of dewatered aquifer was large.

3.6 Foundation pit area effect

The foundation pit area varied from small section of the subway station foundation pit to super large area of industrial and civil buildings. The relationship between 3H drawdown and pit area

is shown in Table **11**. As shown in Fig. **7,** the 3H drawdown decreased with the increase in foundation pit area when other factors remain constant. The foundation pit area had an exponential function to the 3H drawdown. The influence of foundation pit area was more obvious when it was small. The influence gradually weakened and tended to be stable when the foundation pit area exceeded 4000 m^2.

4 Regress model under FPD subsidence control and prevention

4.1 Basic principles of regression analysis

Regression analysis is used to study the quantitative change rule between dependent variable *Y* and independent variable *X* describe its relationship through a certain mathematical expression, and determine the influence degree of one or more independent variables on the dependent variable. A definite functional relationship can be used to approximate the complex correlation. This function is called regression function and is called empirical formula in practical problems. The main problem of regression analysis is the utilization of the observed values (samples) of variables *X* and *Y* to make statistical inferences on regression functions, including their estimation and testing the hypotheses related to them.

In regression analysis, the regression model can be established through nonlinear estimation when the relationship between the independent and dependent variables cannot be simply expressed as a linear equation. In this section, Statistical Product and Service Solutions (SPSS) software was used to establish the regression model on the basis of the principle of nonlinear estimation.

4.2 Multivariate fitting formula for length-to-width ratio

Regression analysis was used to discover the relationship between the 3H drawdown and

length-to-width ratio. The variation basically conformed to an exponential function (Table **12**).

$$D_s = \left(\mathrm{d} + e \times P\right)^k, \tag{10}$$

where P is the length-to-width ratio of the foundation pit (h/w), and d, e, and k are the fitting coefficients.

4.3 Multivariate fitting formula for drawdown outside the pit

The regression variables included W (excavation depth), M (excavation area), and D (depth of diaphragm wall inserted into the aquifer), and the output variable was drawdown. The function model input in the nonlinear regression was expressed as follows:

$$\mathrm{D_s} = (\mathrm{a} \times \mathrm{M} + \mathrm{b} \times \mathrm{W} + \mathrm{c} / \mathrm{D})^{\mathrm{f}} (\mathrm{d} + \mathrm{e} \times \mathrm{P})^{\mathrm{k}}, \tag{11}$$

where D_s is the drawdown of the target aquifer water level at 3H outside the foundation pit (m), D is the depth of diaphragm wall inserted into the target aquifer roof (m), W is the excavation depth of foundation pit (m), M is the foundation pit area (m^2), P is the length–width ratio of foundation pit (length/width), and a, b, c, d, e, f, k, and l are the fitting parameters.

The initial values of the parameters depended on the range of parameters defined in a given model. The Levenberg–Marquardt iteration was used. The maximum iteration step was 100, the change ratio of the residual sum of squares was less than 1×10^{-8}, and the change ratio of parameters was less than 1×10^{-8}.

The parameters and goodness-of-fit coefficients of the regression equation are shown in Table **13**. The narrow and long foundation pit for subway station is shown in Table **14**.

Another regression model is shown as bellow:.

$$P = \left(\alpha \cdot \sqrt{M} + B \cdot W + \frac{c}{\sqrt[3]{D}}\right)^f. \tag{12}$$

The parameters and goodness-of-fit coefficients affecting the distance regression equation are

shown in Table **15**.

During dewatering, multi factors affected the drawdown outside foundation pit. The drawdown curve conforms to the exponential form. The weights of foundation pit depth, diaphragm wall insertion depth, and foundation pit area, influenced the 3H drawdown. Increasing the impact has a weakening trend.

When the length-to-width ratio of the foundation pit was 2:1. The 3H drawdowns of layers ⑤$_2$, ⑦ and ⑨ with different areas, depths, and diaphragm wall depths were analyzed, as shown in Table **16-18** and Fig. **8**.

5 Verification and application

5.1 General situation of the project

Qilianshan South Road Station of Shanghai Rail Transit Line 13 is located at the intersection of Qilianshan South Road and Jinshajiang Road. The main part of its foundation pit is along the east–to–west direction of Jinshajiang Road. The east end well and standard section of the foundation pit is 98, 20 m wide, and 1983 m^2 in area, as shown in Fig. **9**. Its ground surface designed elevation equals to + 3.96 m. The excavation depth of the east end well is 19.501 m. The absolute elevation of diaphragm wall bottom is −31.24 m. The excavation depth of standard section is 17.442 m, and the absolute elevation of diaphragm wall bottom is −27.84 m. The foundation pit is located in the emphasis subsidence prevention zones I1. The dewatered aquifer is the first confined aquifer (layer ⑦). As for SDDC partition, the foundation pit is located in ⑦$_{II1\text{-}2}$ where aquifer layers ⑦ and ⑨ are disconnected (Table **19**).

5.2 Water level verification

Groundwater levels were monitored by observation wells GC2 and GC3 (Fig. **10**) during

435 construction of east end well and standard section. The water level of the two observation wells
436 showed a consistent trend and close to the numerical simulations (Fig. **11**). The calculated
437 drawdown was greater than the monitored one because the influence of monitoring location.
438 The FPD numerical simulation conformed to the actual geological conditions. The calculation
439 results were accurate and effective.

440 **5.3 Land subsidence verification**

441 The cumulative land subsidence of the north and east sections of the foundation pit are shown
442 in Fig. **12**.

443 As shown in Fig. **13,** the subsidence monitoring results of the north side are close to the
444 calculation results, and the observation section on the south side deviates from the actual
445 monitoring values because of the increase in the excavation depth of the end well foundation
446 pit and the increase in the insertion depth of the diaphragm wall.

447 The above analysis shows that the calculation method of FPD land subsidence caused by is
448 reasonable. This method can accurately predict the ground subsidence caused by FPD and
449 can be used to predict the land subsidence caused by FPD outside the pit (Tables **20**).

450 **6 Conclusions**

451 FPD land subsidence evaluation and control indicators were defined. On the basis of cases
452 collection and characteristic estimation, the FPD conceptual was established. A total of 6540
453 FPD numerical simulations were performed under SDDC partitions. Regress method was
454 introduced to evaluate the 3H drawdown to control FPD land subsidence. The following
455 conclusions were obtained:

456 (1) The maximum 3H land subsidence was defined as the evaluation indicator of FPD land

subsidence, and the maximum 3H drawdown corresponding to 3H subsidence was defined as control indicator.

(2) FPD conceptual models based on Landform, LSPC and SDDC partitions established can describe common 3H FPD drawdown and land subsidence. The FPD drawdown funnel outside pit can be divided into steep change, slow change, and residual zones.

(3) Multiple regression model was established to obtain 3H drawdown on the basis of pit shape, pit depth, pit area, and cutoff depth. The model can be used to predict FPD 3H drawdown and evaluate whether the corresponding land subsidence can satisfy the evaluation indicator of 3H land subsidence.

(4) The accuracy and effectiveness of the regress models were verified by using the water level monitoring data of Qilianshan South Road Station of Shanghai Rail Transit Line 13.

(5) The regress model can be used in land subsidence prevention and control in Shanghai. The methods can also provide reference for other similar lowland coastal cities.

Acknowledgements

This research was funded by the Shanghai Municipal Science and Technology Project (18DZ1201301; 19DZ1200900); Key Laboratory of Land Subsidence Monitoring and Prevention, Ministry of Natural Resources of the People's Republic of China (No. KLLSMP202101); Shanghai Municipal Science and Technology Major Project (2021SHZDZX0100) and the Fundamental Research Funds for the Central Universities; the project of Key Laboratory of Impact and Safety Engineering (Ningbo University), Ministry of Education (CJ202101); Xiamen Road and Bridge Group (XM2017-TZ0151; XM2017-TZ0117);,

Suzhou Rail Transit Line 1 Co. Ltd; China Railway 15 Bureau Group Co. Ltd.; IGCP Project [grant number 663-La Subsidence in Coastal cities].

References

Nicoleta C., Cristian R., Ioan B., 2017. Dewatering system of a deep of excavation in urban area – bucharest case study. Proced. Eng. 209, 210–215. https://doi.org/10.1016 /j.proeng.2017. 11.149.

Chen C., Pei S., Jiao J., 2003. Land subsidence caused by groundwater exploitation in Suzhou city, china. Hydrogeol. J. 11, 275-287.

Khosravi, M., Khosravi, M.H., & Najafabadi, S.H.G., 2018. Determining the portion of dewatering-induced settlement in excavation pit projects. Int. J. Geotech. Eng. 209, 210-215.

Luo, Z.J., Liu, J.B., Zhang, Y.P. et al., 2006. Three dimensional coupled numerical model between deep foundation pit dewatering and land–subsidence. J. Jiangsu Univ. (Natural Science Edition). 27, 356-359. (in Chinese)

McDonald M.G. and Harbaugh A.W., A modular three-dimensional finite-difference ground-water flow model, U.S. Geological Survey, Techniques of Water-Resources Investigations, Book 6, Chapter A1 .United states Government Printing Office. Washington.

Miyake N., Kohsaka N., Ishikawa A., 2008. Multi-aquifer pumping test to determine cutoff wall length for groundwater flow control during site excavation in Tokyo, Japan. Hydrogeol J. 16, 995–1001. https://doi.org/10.1007/s10040-008-0276-3

Mo Y.T., Fu B.J., 2002. Design and application of combined system of deep well and reinjection well in complex deep foundation pit. Chin. Overseas Architect. 84-85. (in Chinese)

501 Hoque, M.A., Hoque, M.M., Ahmed, K.M., 2007. Declining groundwater level and aquifer
502 dewatering in Dhaka metropolitan area, Bangladesh: causes and quantification. Hydrogeol.
503 J. 15, 1523-1534.
504 Shen S.L.,Wu Y.X., Sun W.J. et al., 2012. Groundwater control for a deep excavation pit in
505 gravel aquifer of Hangzhou, China. In: Proceedings of the International Conference on Ground
506 Improvement and Ground Control,1735-1745. 10.3850/978-981-07-3560-9_10-1015.
507 Shi Y.J., Li M.G., Zhang Y.Q. et al., 2018. Field investigation and prediction of responses of far-
508 field ground and groundwater to pumping artesian water in deep excavations. Int. J.
509 geomech. 18, 04018132.1-04018132.12.
510 Wang J., Hu L., Wu L. et al., 2009. Hydraulic barrier function of the underground continuous
511 concrete wall in the pit of subway station and its optimization. Environ. Geol. 57, 447–453.
512 https://doi.org/10.1007/s00254-008-1315-z
513 Wang J., Feng B., Yu H. et al., 2013. Numerical study of dewatering in a large deep foundation
514 pit. Environ. Earth. Sci. 69, 863–872. https://doi.org/10.1007/s12665-012 -1972-9.
515 Wang J., Feng B., Guo T.P. et al., 2013. Using partial penetrating wells and curtains to lower
516 the water level of confined aquifer of gravel. Eng. Geol. 161, 16–25. 10.1016/j.enggeo.
517 2013.04.007.
518 Wang J., Huang T., Hu J. et al., 2014. Field experiments and numerical simulations of whirlpool
519 foundation pit dewatering. Environ. Earth. Sci. 71, 3245–3257. https://doi.org/10. 1007/
520 s12665-013-2981-z
521 Wang J., Liu X., Liu S. et al., 2019. Physical model test of transparent soil on coupling effect of
522 cut-off wall and pumping wells during foundation pit dewatering. Acta Geotech. 14, 141–162.

https://doi.org/10.1007/s11440-018-0649-2

Wang J., Liu X., Liu J. et al., 2018. Dewatering of a 32.55 m deep foundation pit in MAMA under leakage risk conditions. KSCE J. Civ. Eng. 22, 2784–2801. https://doi.org/10.1007/s12205- 017-1950-6

Wang J., Wu Y., Liu X. et al., 2016. Areal subsidence under pumping well–curtain interaction in subway foundation pit dewatering: conceptual model and numerical simulations. Environ. Earth. Sci. 75, 198.1-198.13. https://doi.org/10.1007/s12665-015-4860-2

Wang Z., Wang C., 2019. Analysis of deep foundation pit construction monitoring in a metro station in Jinan City. Geotech. Geol. Eng. 37, 813–822. https://doi.org/10.1007/s10706-018-0651-3

Hung W., Hwang C., Chang C. et al., 2010. Monitoring severe aquifer-system compaction and land subsidence in Taiwan using multiple sensors: Yunlin, the southern Choushui River Alluvial Fan. Environ. Earth. Sci. 59, 1535–1548. https://doi.org/10.1007/s12665-009 -0139-9

Wu J., Shi X., Ye S. et al., 2009. Numerical simulation of land subsidence induced by groundwater overexploitation in Su-Xi-Chang area, China. Environ. Geol. 57, 1409–1421. https://doi.org/10.1007/s00254-008-1419-5

Wu Y.X., Shen S.L., Xu Y.S. et al., 2015. Characteristics of groundwater seepage with cut-off wall in gravel aquifer. I: Field observations. Can. Geotech. J. 52,10.1139/cgj-2014-0285, ,

Wu Y.X., Shen S.L., Yin Z.Y. et al., 2015. Characteristics of groundwater seepage with cut–off wall in gravel aquifer. II: Numerical analysis. Can. Geotech. J. 52,10, 150223161106004.10.1139/cgj-2014-0289

Zeng, C.F., Zheng, G., Xue, X.L. et al., 2018. Combined recharge: A method to prevent ground

545 settlement induced by redevelopment of recharge wells. J. Hydrol. 568, 1–
546 11.1016/j.jhydrol.2018.10.051.
547 Zhang Y., Xue Y., Wu J. et al., 2010. Excessive groundwater withdrawal and resultant land
548 subsidence in the Su-Xi-Chang area, China. Environ. Earth. Sci. 61, 1135–1143.
549 https://doi.org/10.1007/s12665-009-0433-6
550 Zhang Y.Q., Wang J.H., Li M.G., 2018. Effect of dewatering in a confined aquifer on ground
551 settlement in deep excavations. Int. J. Geomech. 18. 10.1061/(ASCE)GM.1943-5622.0001233.
552 Shanghai Construction Material Industry Market Management Station (SHCMIMMS). 2018.
553 Code for construction of shanghai municipal engineering. Technical code for excavation
554 engineering, DG/TJ08-61-2018.
555 Shanghai Construction Material Industry Market Management Station (SHCMIMMS). 2018.
556 Technical code for land subsidence monitor and control. Technical code for excavation
557 engineering, DG/TJ08-2051-2008.
558

Figures

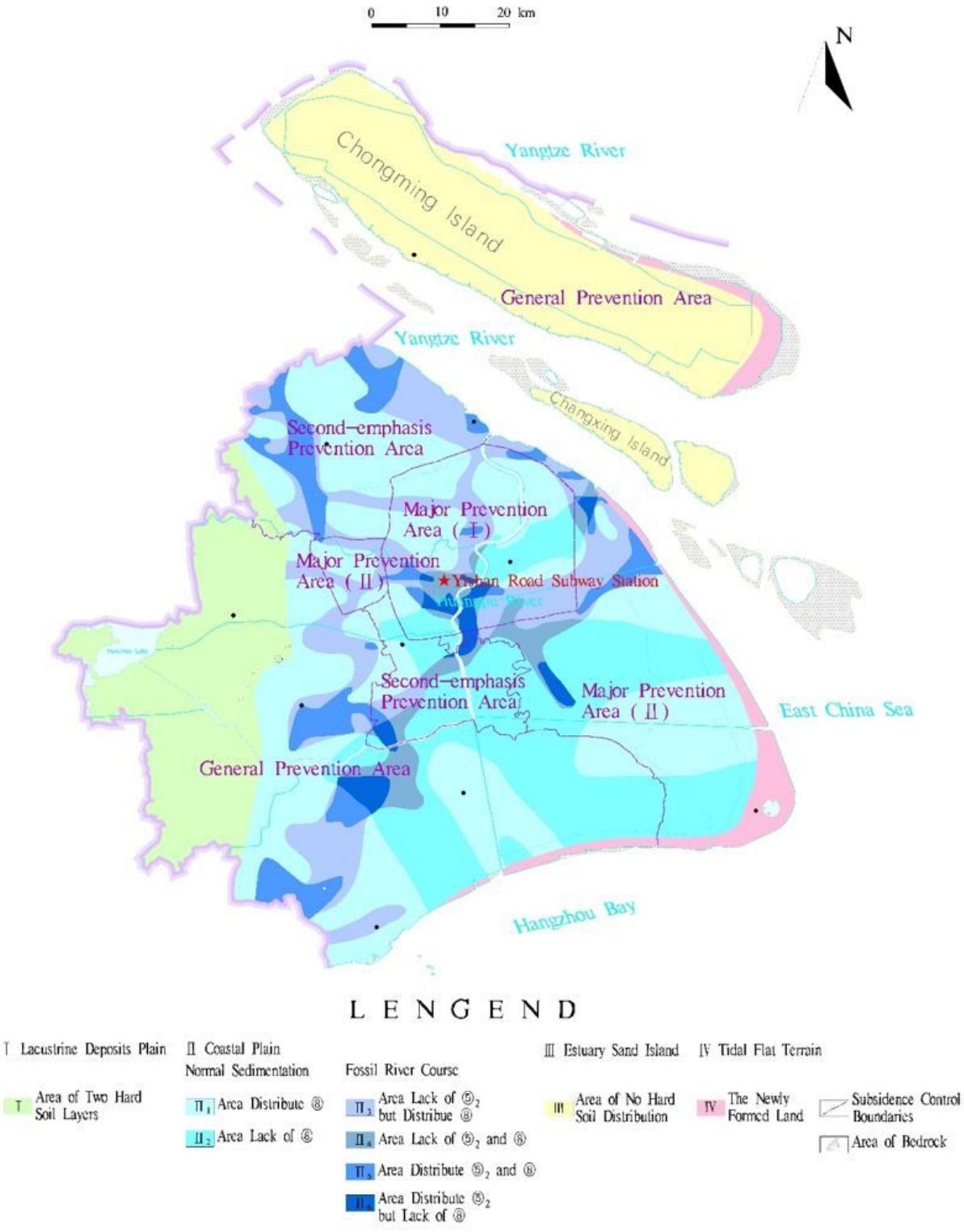

Figure 1

LSPC partitions of Shanghai

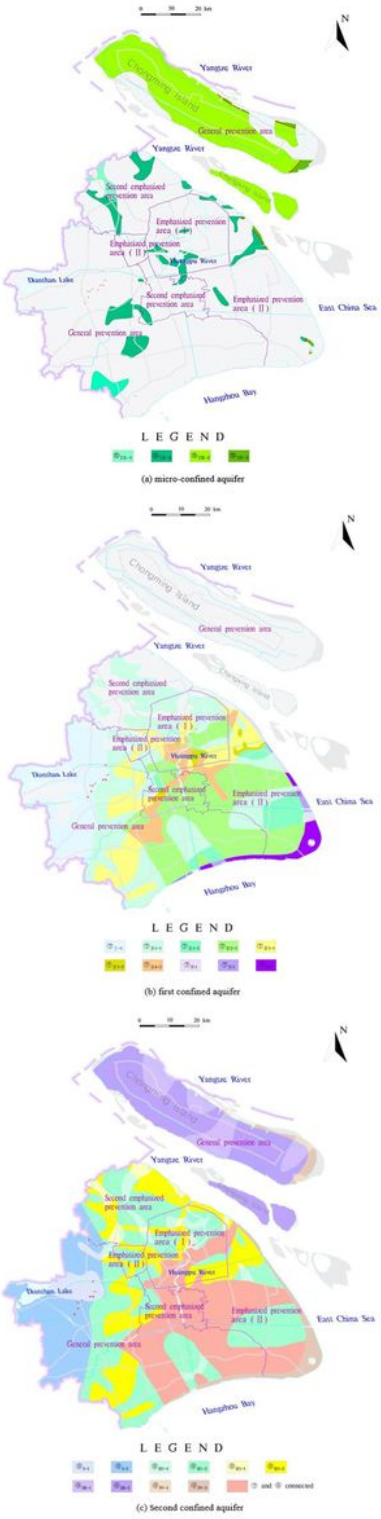

Figure 2

SDDC partition for confined aquifers of Shanghai

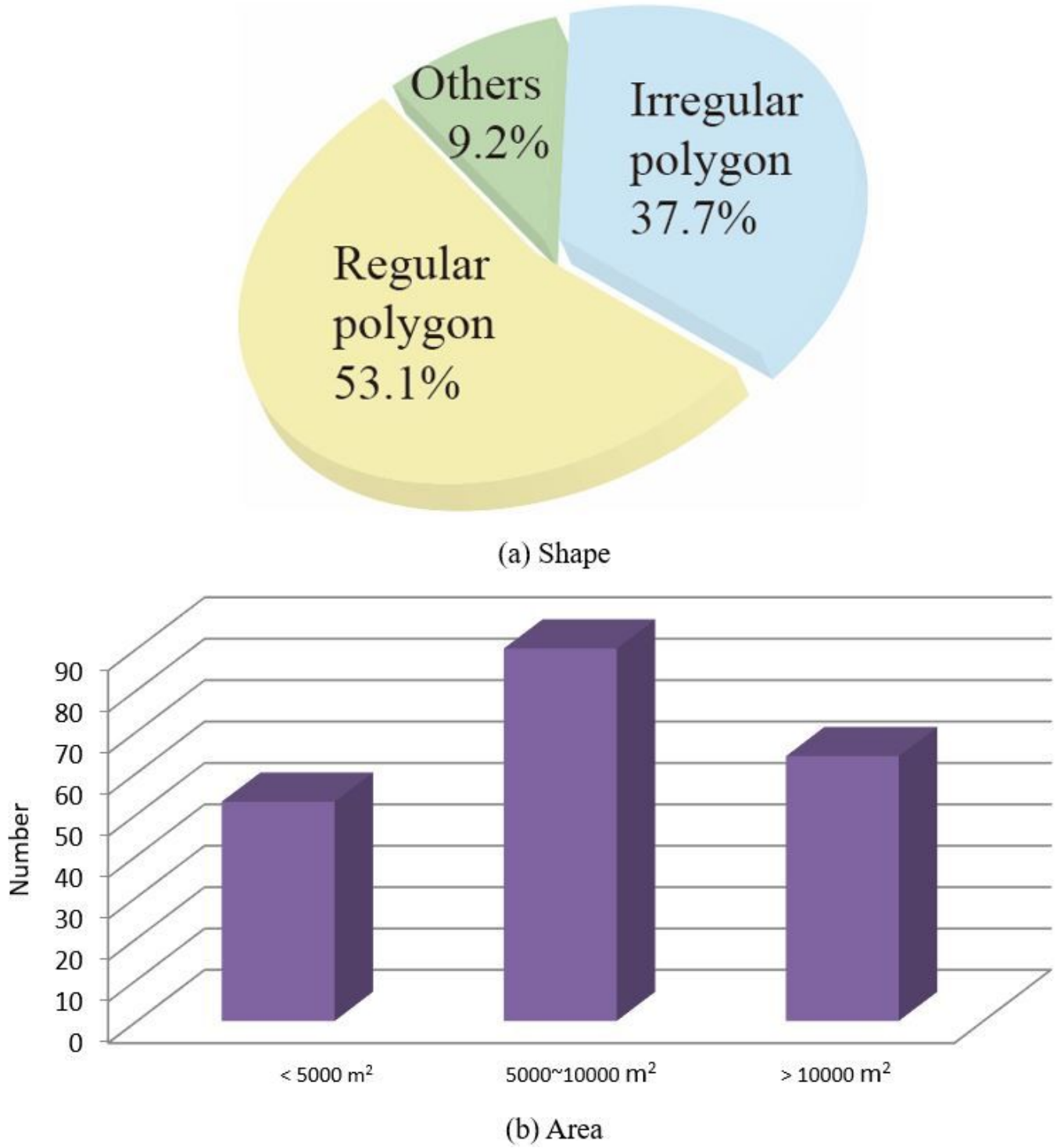

Figure 3

Estimation of foundation pit information in Shanghai

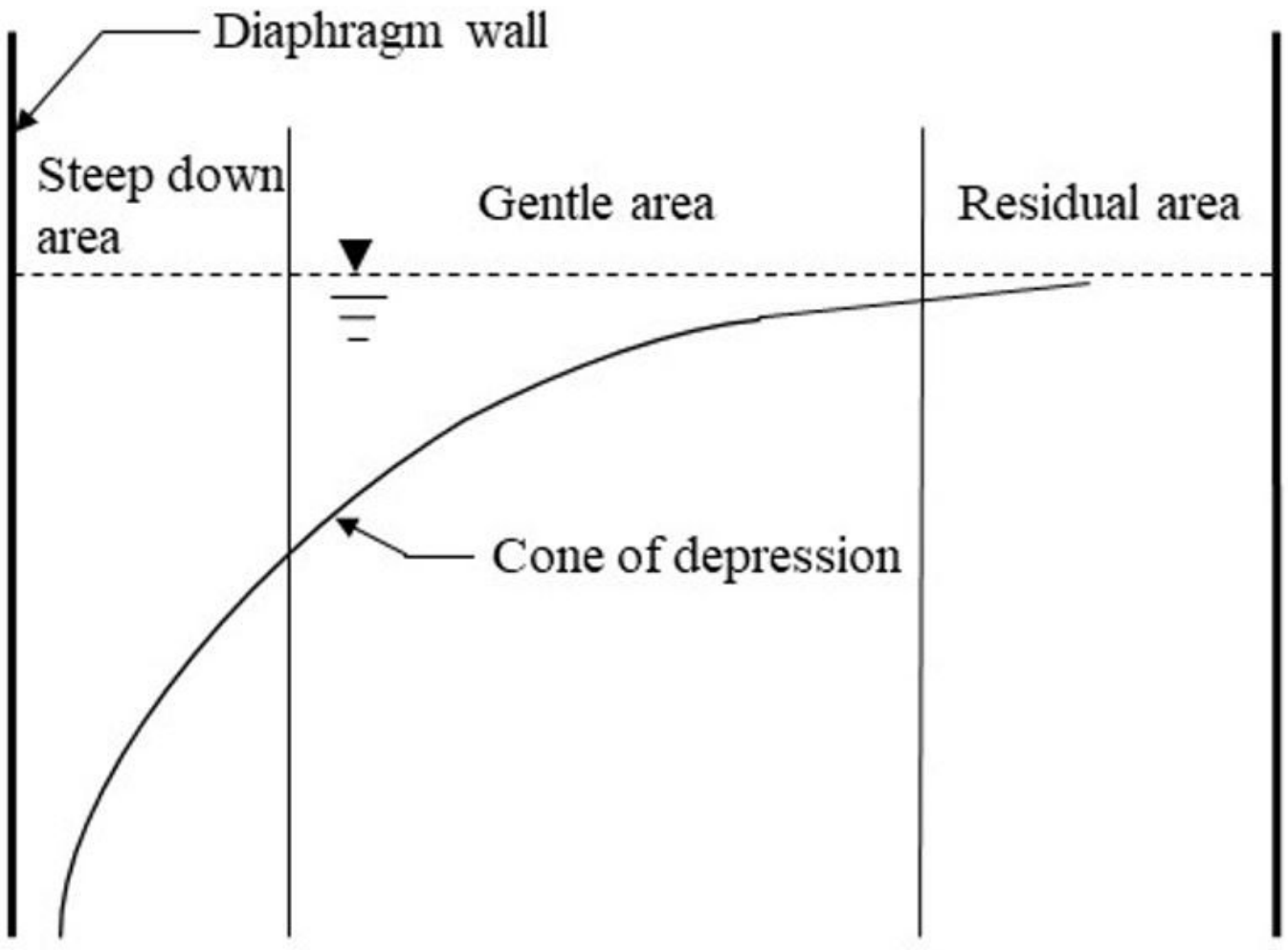

Figure 4

Zoning of a drawdown funnel

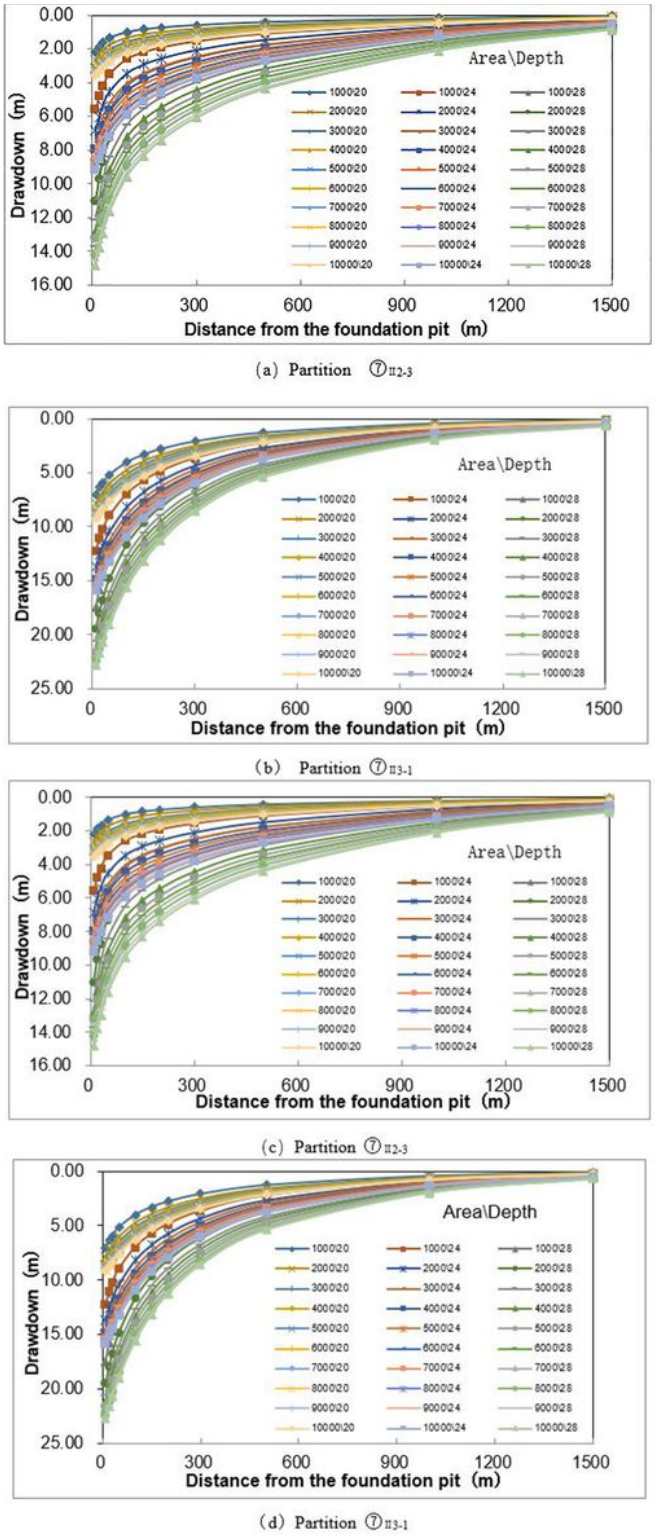

Figure 5

Drawdown-distance curve for different area and depth when cutoff depth is 5m

(Legend indicate pit area\depth)

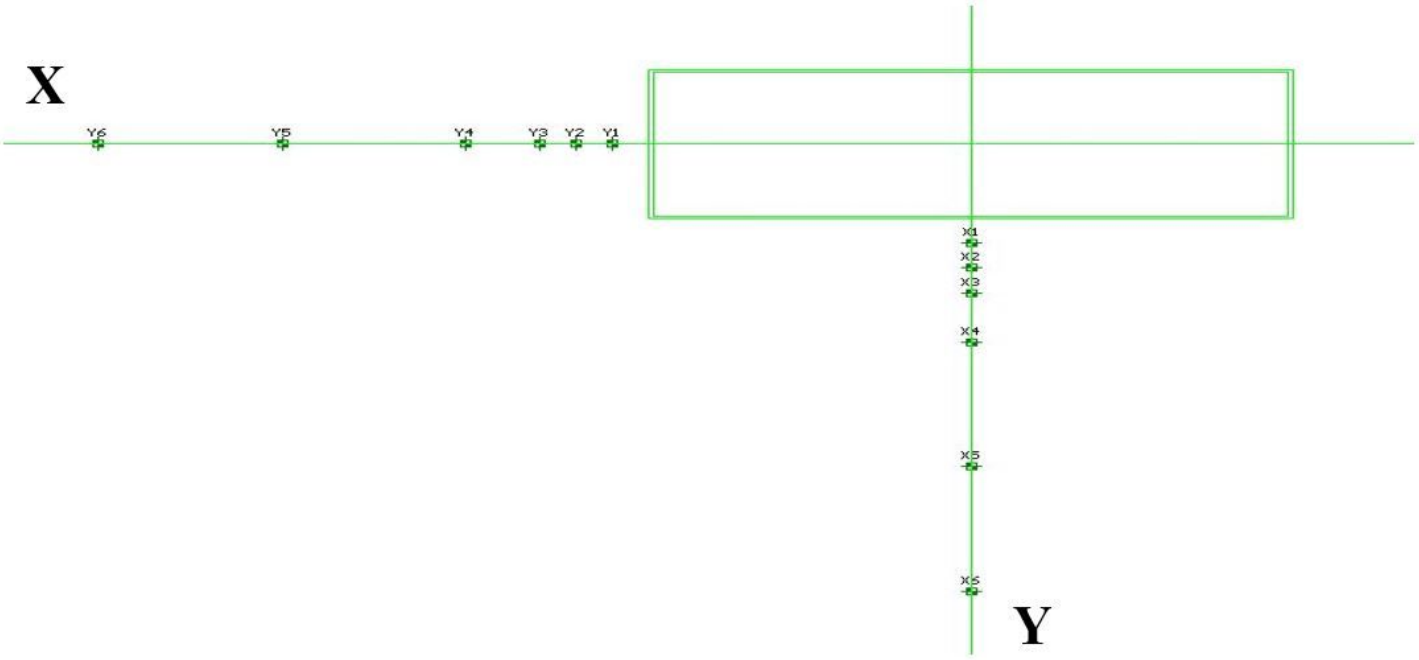

Figure 6

Layout of observation well in X and Y directions in calculations

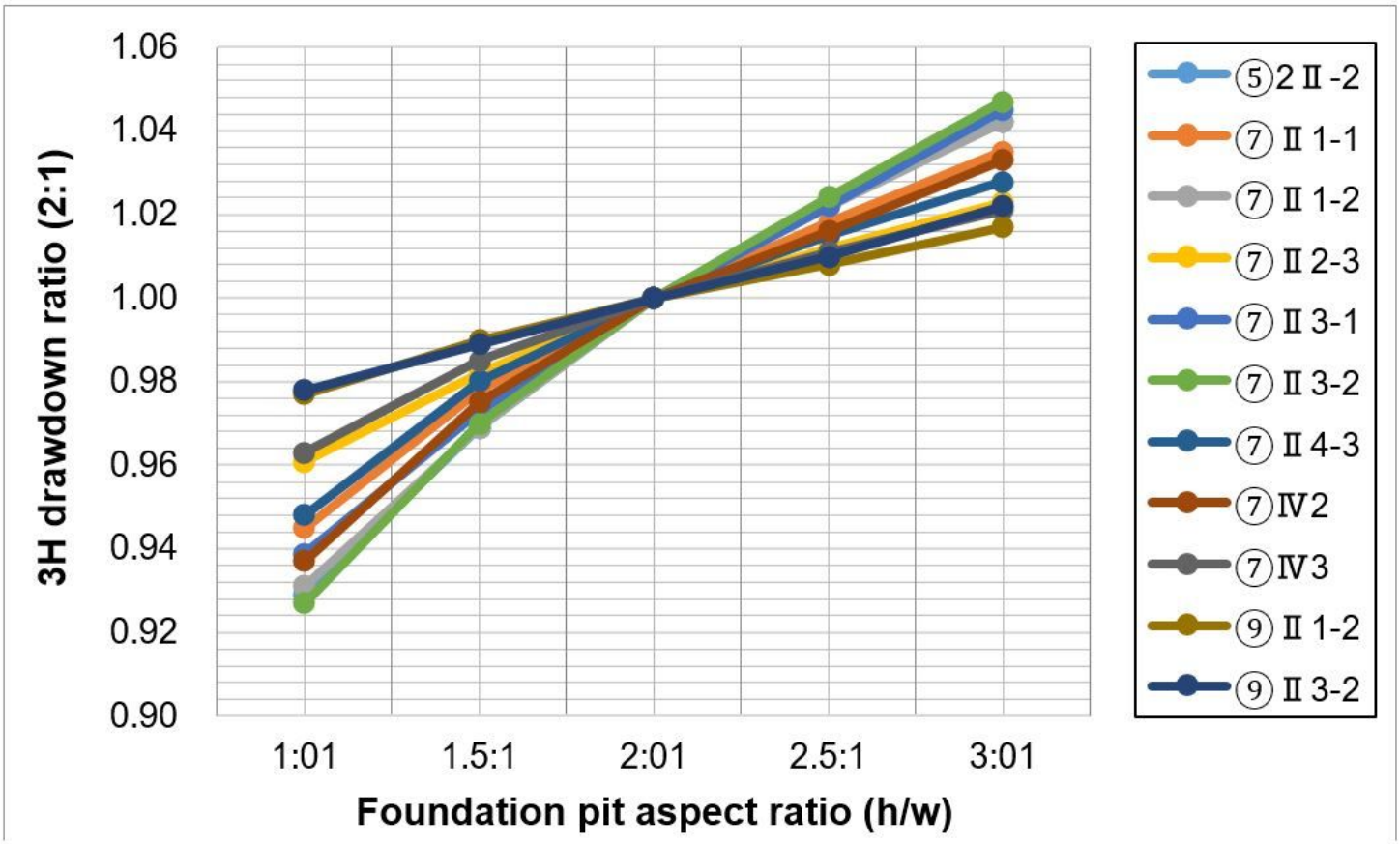

Figure 7

Influence of length/width ratio to drawdown

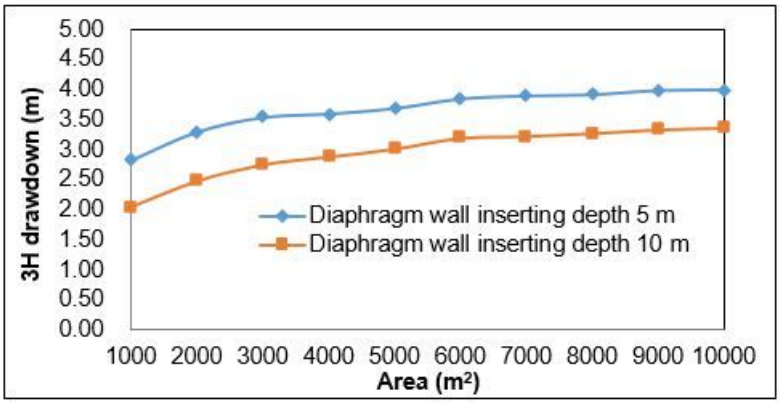

(a) Influence of pit area on drawdown in partition ⑤$_{2Ⅱ6-2}$ when length width ratio is 2:1; pit depth is 16m

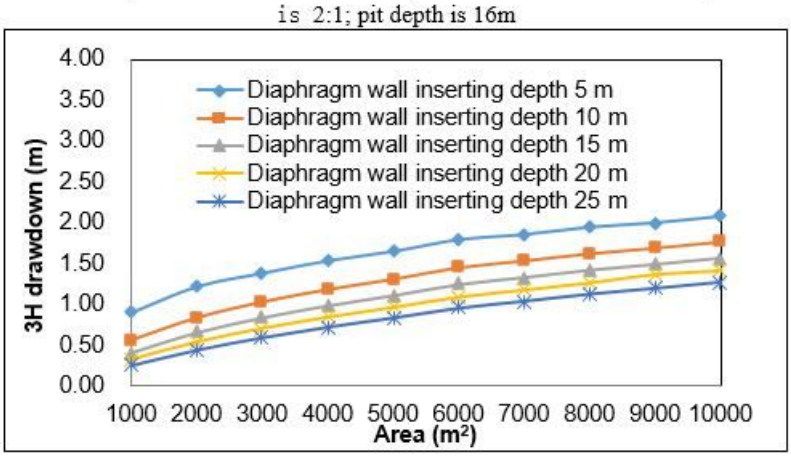

(b) Influence of pit area on drawdown in partition ⑦$_{Ⅱ4-3}$ when length/width ratio is 2:1; pit depth is 20 m

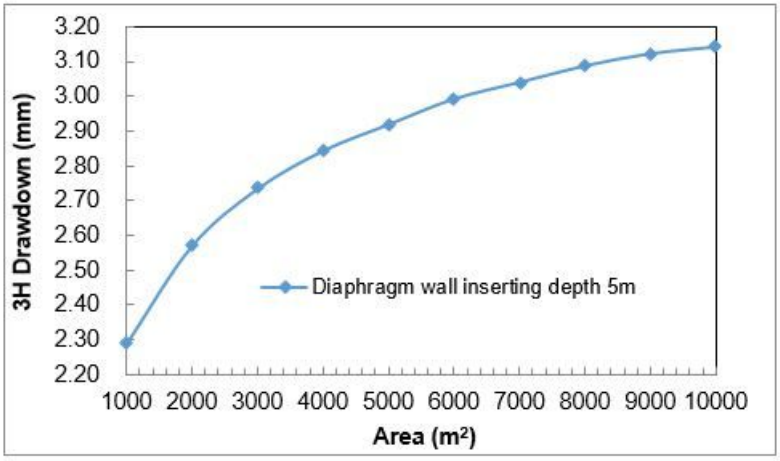

(c) Influence of pit area on drawdown in partition ⑨$_{Ⅱ1-2}$ when length/width ratio is 2:1; pit depth is 32 m

Figure 8

Influence of foundation pit area on drawdown

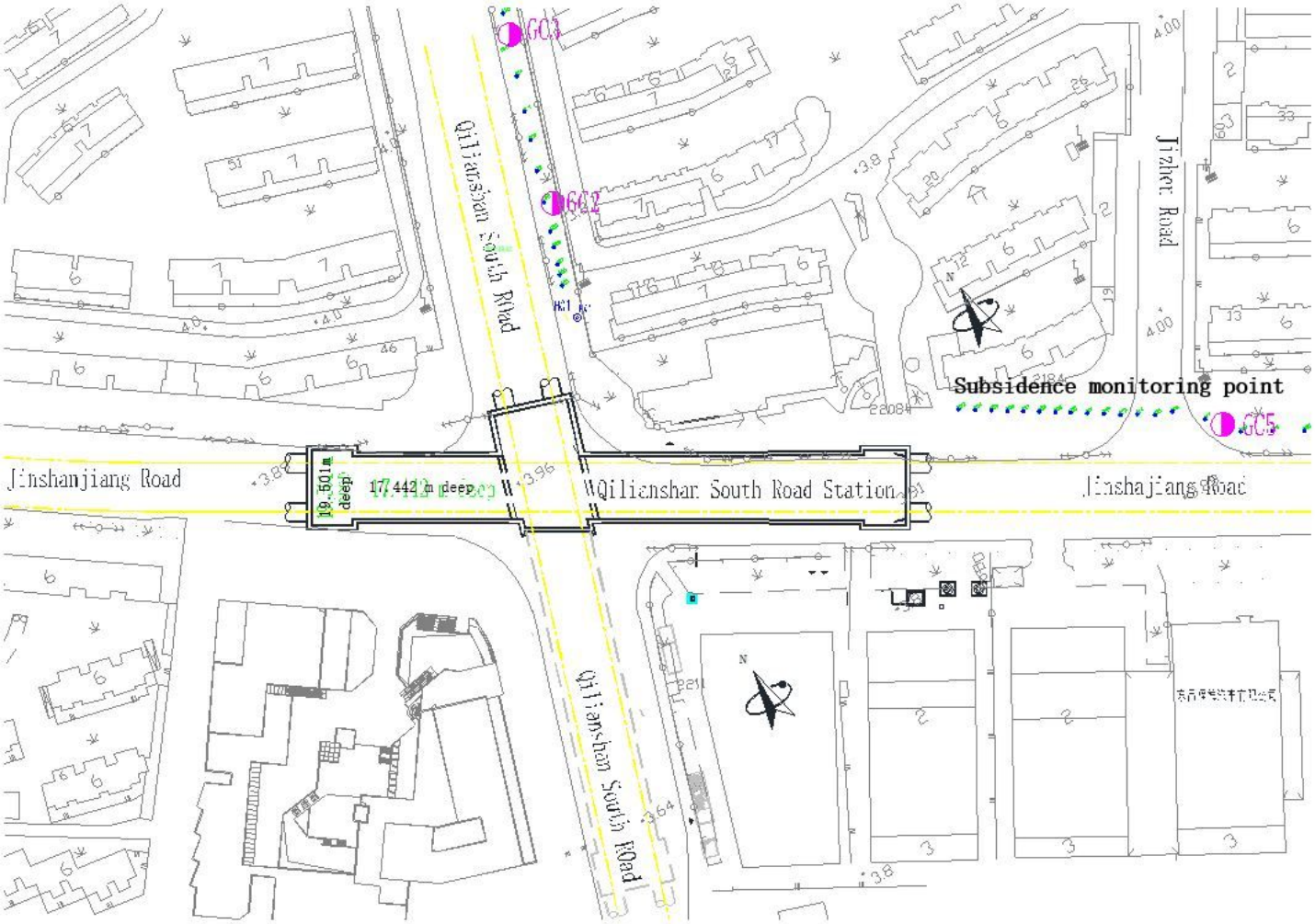

Figure 9

Plane arrangement of Qilianshan South station foundation pit of Line 13, Shanghai metro

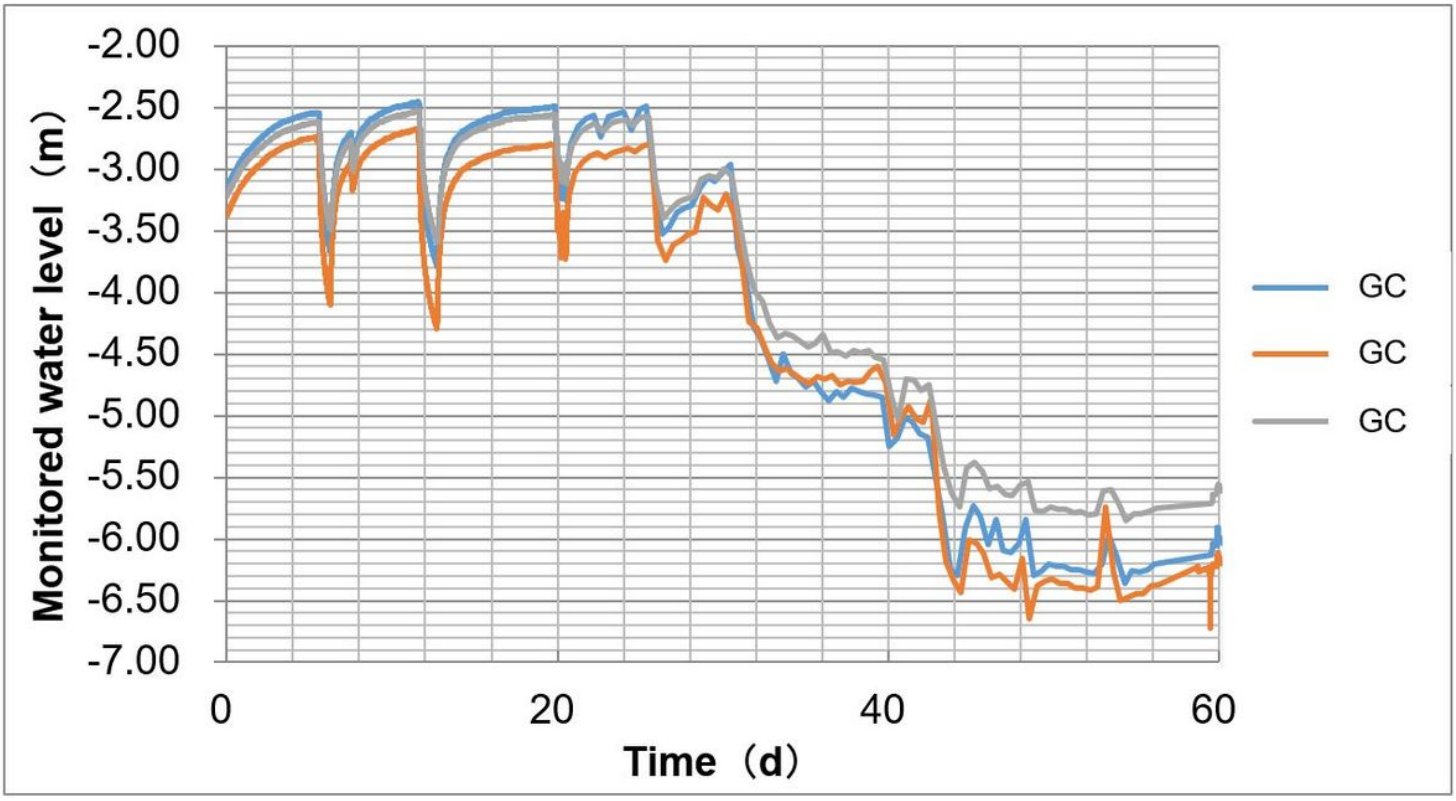

Figure 10

Drawdown-time curve in observation well outside foundation pit

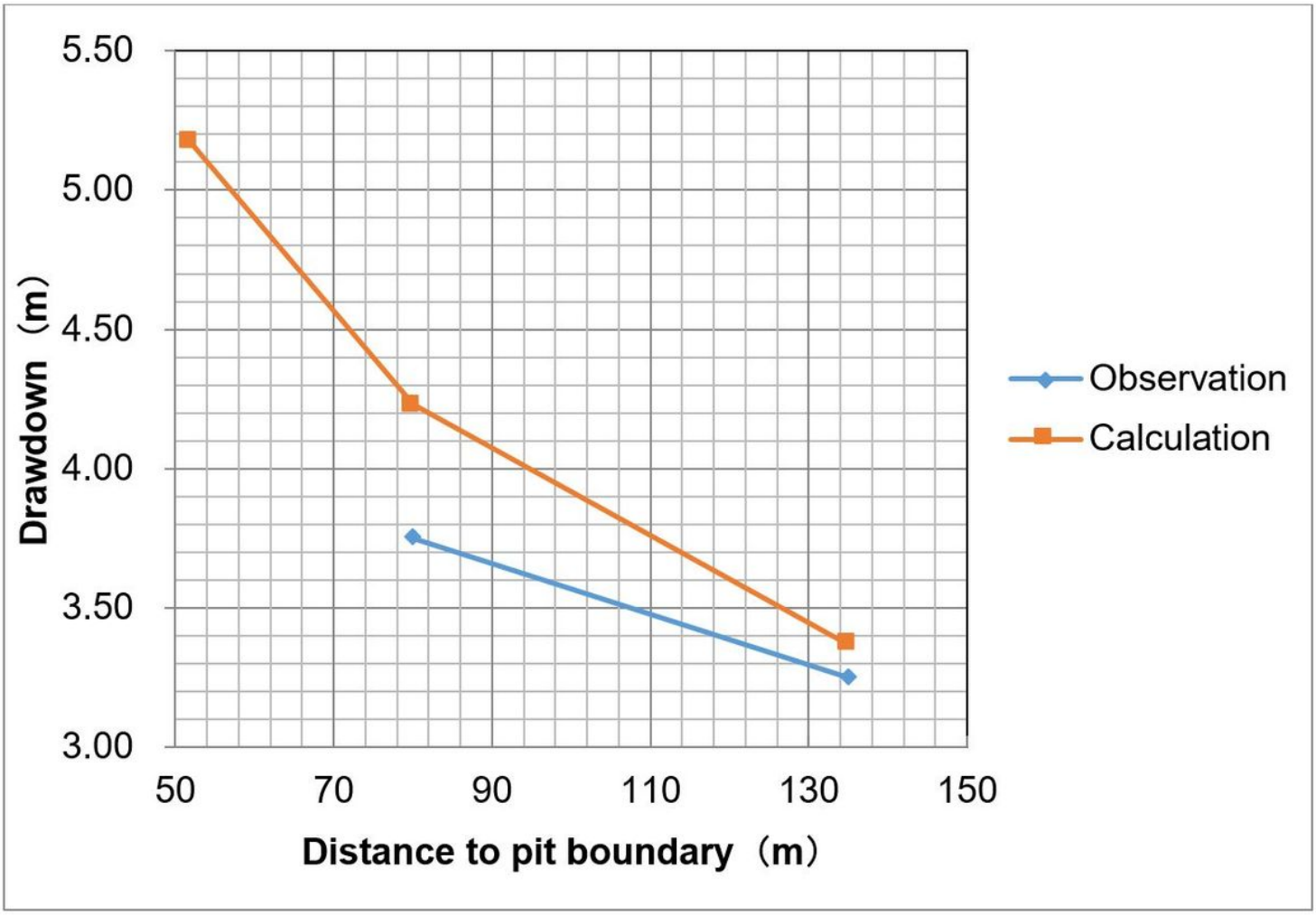

Figure 11

Comparison between monitoring and calculation

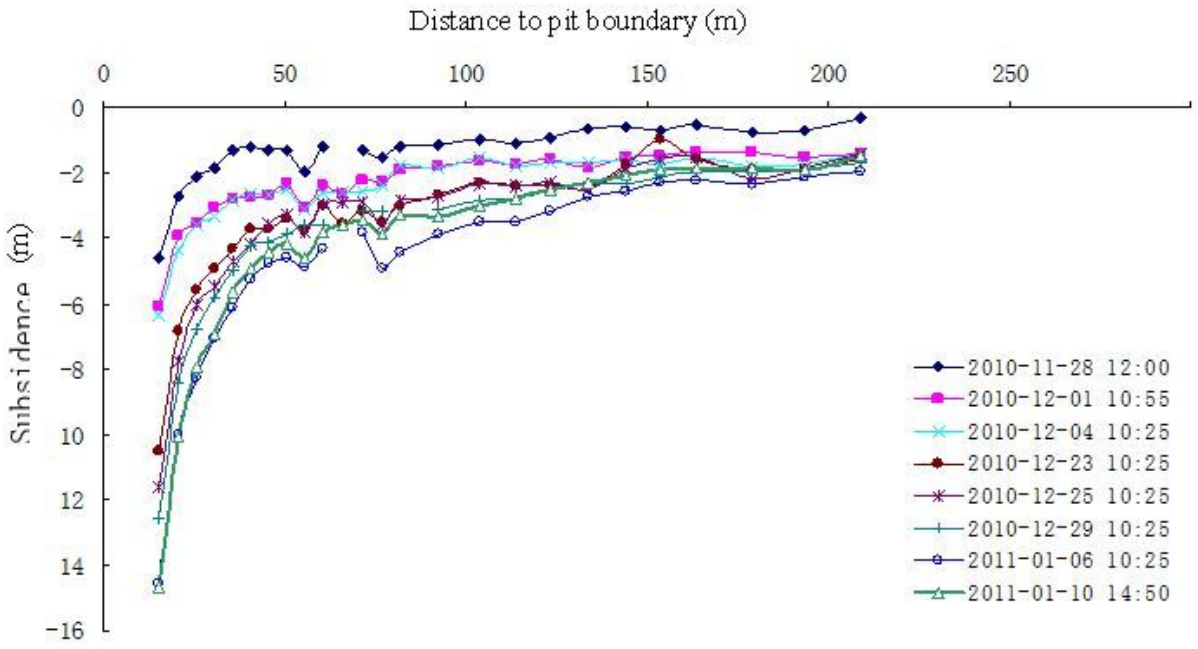

(a) north of foundation pit

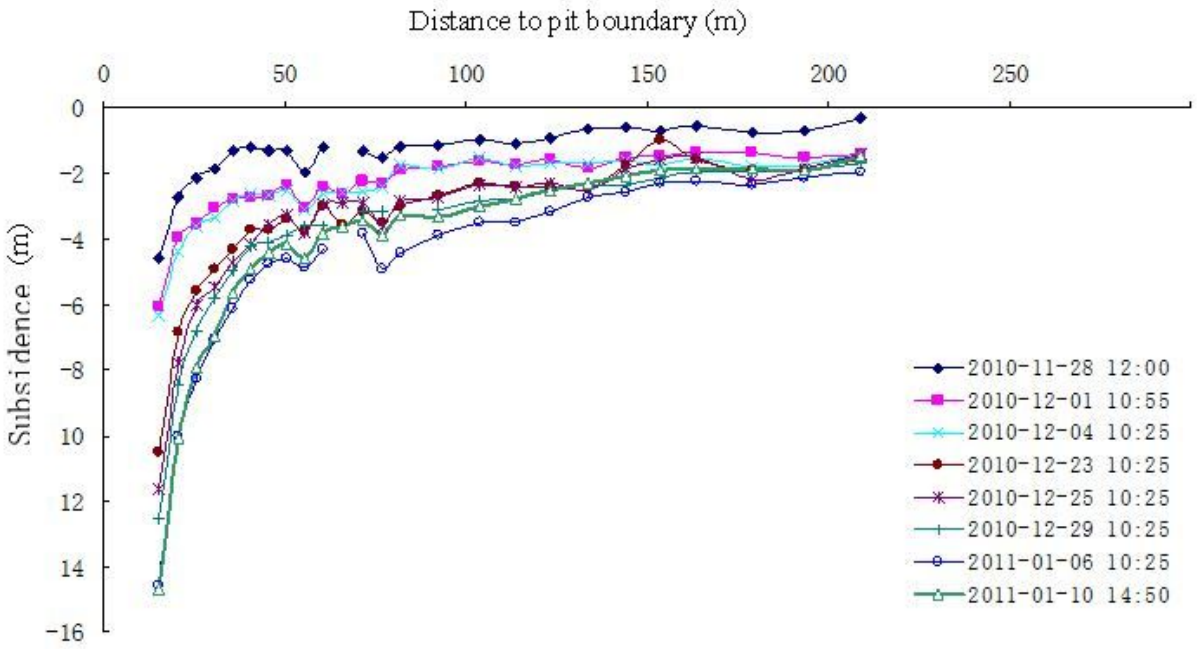

(b) east of foundation pit

Figure 12

Accumulation subsidence in the east of foundation pit

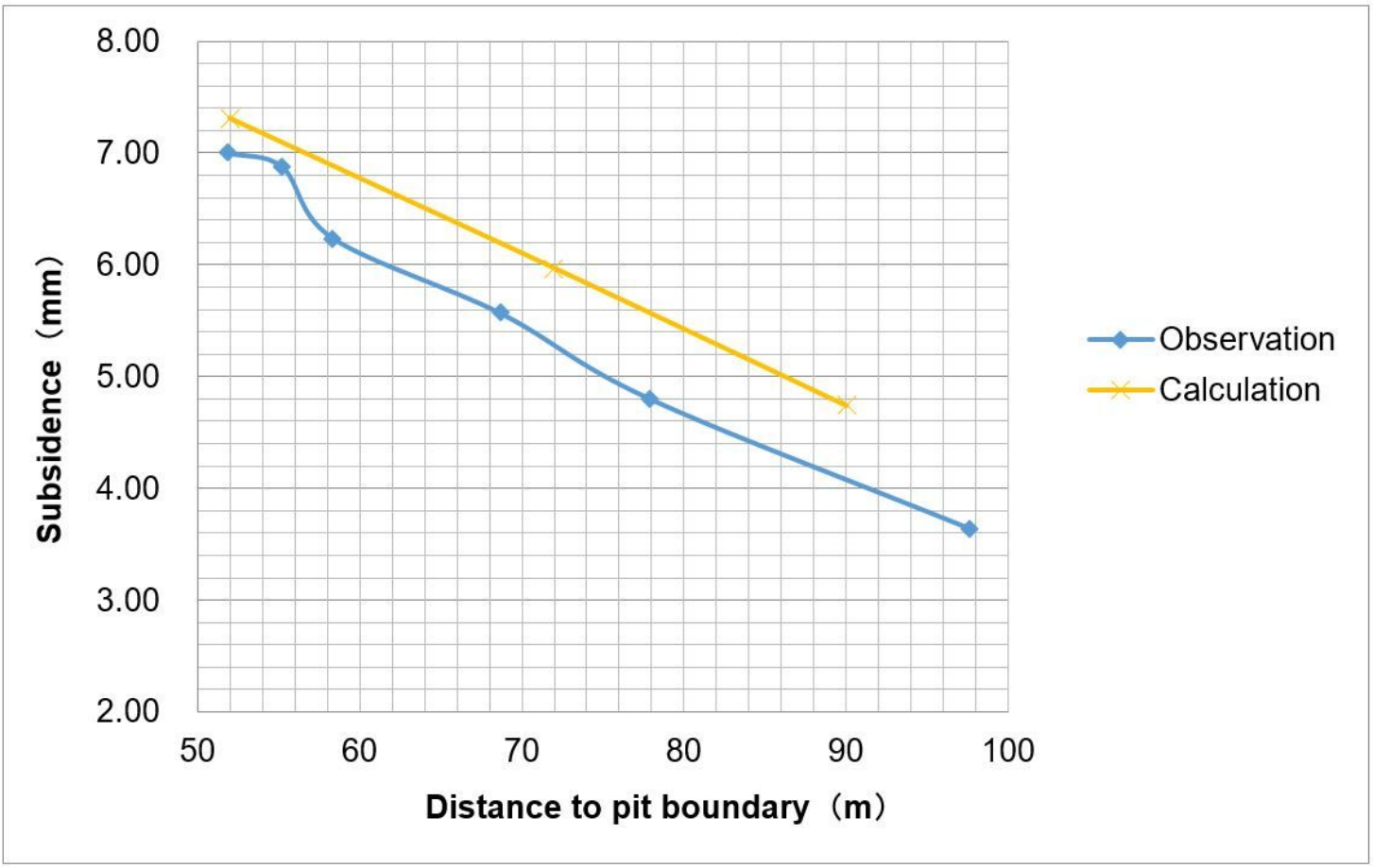

Figure 13

Comparison of subsidence between monitoring and calculation in north of pit